symmetry

MDPI

Article

Construction of a New Distribution Based on the Standardized Student-t Distribution and Its Application

Jingjie Yuan and Zuoquan Zhang *

School of Mathematics and Statistics, Beijing Jiaotong University, Beijing 100044, China; 22110498@bjtu.edu.cn
* Correspondence: zuoquanzhang@163.com

Abstract

We propose a flexible framework for modeling financial returns using orthogonal expansions of the standardized Student-t density. The Skew-Kurtotic t Expansion (SKTE) captures skewness and excess kurtosis while preserving heavy tails. Orthogonal polynomials are constructed with the t kernel, while a fourth-order truncation provides a parsimonious and interpretable parameterization. Squaring and normalization ensure a valid density. Truncation accuracy analysis shows that the fourth-order approximation balances computational efficiency and tail fidelity, with higher-order terms offering minimal improvement. Empirical analysis of daily returns for the Hang Seng Index, S&P 500, front-month natural gas futures, and EUR/USD exchange rate shows that SKTE outperforms the classical Gram–Charlier expansion, particularly in tail modeling. Maximum likelihood estimation confirms stable skewness and kurtosis adjustments, while location and scale parameters align the distribution to each asset. These results indicate that SKTE provides a robust and flexible framework for modeling asymmetric and heavy-tailed stock return distributions, which is highly relevant for understanding extreme market behavior.

Keywords: Gram–Charlier expansion; asymmetry and heavy tails; standardized Student-t distribution; orthogonal polynomial; stock return

MSC: 62P05; 91G70; 60E05

1. Introduction

Accurately modeling the distribution of financial asset returns is essential for risk management, derivative pricing, and portfolio optimization. Empirical evidence indicates that asset returns often deviate from normality, exhibiting skewness, excess kurtosis, and heavy tails [1–7]. These deviations are particularly pronounced in high-frequency returns, where extreme movements and asymmetries can lead to substantial underestimation of risk if standard normal-based models are employed [8,9]. Consequently, accurate modeling of both skewness and kurtosis is critical for capturing tail risk, computing Value-at-Risk (VaR), and pricing options and other derivatives.

The Gram–Charlier series expansion of the normal density function provides a convenient framework to incorporate higher-order moments directly into the probability density [10–13]. However, densities derived from this expansion frequently fail to capture the skewness and kurtosis observed in daily or intraday returns. Moreover, certain skewness–kurtosis combinations can produce negative or multimodal densities that compromise validity [14]. Analytical [15] and numerical [16,17] studies have partially addressed

Check for updates

Academic Editors: Junesang Choi and Marek T. Malinowski

Received: 5 December 2025
Revised: 1 February 2026
Accepted: 3 February 2026
Published: 6 February 2026

Copyright: © 2026 by the authors. Licensee MDPI, Basel, Switzerland. This article is an open access article distributed under the terms and conditions of the Creative Commons Attribution (CC BY) license.

this issue by identifying ranges of skewness and kurtosis that preserve positivity. For standardized variables with mean zero and unit variance, skewness between -1 and 1 and kurtosis between 3 and 7 yield approximately 71–90% of positive expansions, which may suffice for lower-frequency returns but is inadequate for high-frequency data.

To overcome these limitations, flexible alternatives have been proposed. The skew-normal and related families extend symmetric distributions to incorporate asymmetry [18], while heavy-tailed distributions such as the Student-t distribution capture extreme events but lack flexibility in modeling skewness. The Gram–Charlier expansion has also been widely applied in econometric and financial contexts [19–23], for instance in modeling conditional densities in GARCH frameworks [22] as well as in estimating time-varying volatility, skewness, and kurtosis [23]. Nevertheless, capturing high-frequency return behavior remains challenging, motivating the development of distributions that simultaneously allow for skewness, kurtosis, and heavy tails.

In this paper, we propose a flexible expansion of the standardized Student-t distribution, introducing parameters μ_3 and μ_4 that are associated with third- and fourth-order shape characteristics of the distribution. This Skew-Kurtotic t Expansion (SKTE) explicitly models skewness and excess kurtosis while preserving the heavy-tailed nature of the t distribution.

Orthogonal polynomials are constructed with respect to the standardized Student-t density, regarded as a finite-order weight function, while a fourth-order truncation provides a parsimonious and interpretable parameterization. Squaring and normalization ensure a valid probability density, while truncation accuracy analysis demonstrates that the chosen order balances computational efficiency and tail fidelity. Empirical applications to daily returns of the Hang Seng Index, S&P 500, front-month natural gas futures, and EUR/USD exchange rate show that SKTE outperforms classical Gram–Charlier expansions in capturing tail behavior and in flexibly adjusting skewness and kurtosis.

The remainder of the paper is organized as follows: Section 2 verifies that the standardized Student-t density can serve as a finite-order weight function for orthogonal polynomial expansions; Section 3 develops the corresponding orthogonal expansion framework, including the general form and an analysis of truncation accuracy; Section 4 presents an empirical comparison of distributional models using historical financial returns; finally, Section 5 concludes with a summary of the main findings and a discussion of potential extensions.

2. Verification that the Standardized Student-t Density Is a Finite-Order Weight Function

A commonly used family for controlling tail thickness is the Student-t family. The Probability Density Function (PDF) of a Student-t variable X is

$$f(x;\nu) = \frac{\Gamma\left(\frac{\nu+1}{2}\right)}{\sqrt{\nu\pi}\,\Gamma\left(\frac{\nu}{2}\right)}\left(1+\frac{x^2}{\nu}\right)^{-\frac{\nu+1}{2}},$$

where ν is the degrees of freedom. Its mean is 0 and variance is $\nu/(\nu-2)$ (for $\nu > 2$).

The PDF of the standardized Student-t variable $T = \dfrac{X}{\sqrt{\nu/(\nu-2)}}$ is

$$t(x;\nu) = \frac{\Gamma\left(\frac{\nu+1}{2}\right)}{\sqrt{(\nu-2)\pi}\,\Gamma\left(\frac{\nu}{2}\right)}\left(1+\frac{x^2}{\nu-2}\right)^{-\frac{\nu+1}{2}}, \quad x \in \mathbb{R}, \tag{1}$$

which has mean 0 and unit variance. For finite ν, the tails of $t(x;\nu)$ are heavier than the normal.

https://doi.org/10.3390/sym18020301

To prepare for the orthogonal polynomial construction used later, we first introduce the notion of a weight function. Specifically, we recall the classical definition of a weight function and then clarify a finite-order variant that is sufficient for the truncated polynomial expansions considered in this paper. Within this finite-order framework, we verify that the standardized Student-t density satisfies the required conditions.

Lemma 1. *Let $[a,b]$ be a finite or infinite interval and let the non-negative function $\rho(x)$ on $[a,b]$ satisfy the following:*

1. *The integral $\int_a^b x^k \rho(x)\,\mathrm{d}x$ exists and is finite for all integers $k \geq 0$.*
2. *For any non-negative continuous function $g(x)$ on $[a,b]$, if $\int_a^b g(x)\rho(x)\,\mathrm{d}x = 0$, then $g(x) \equiv 0$.*

Then, $\rho(x)$ is called a weight function on $[a,b]$ (for further details, see Li et al. [24]).

The above definition corresponds to the classical infinite-order notion of a weight function. However, the orthogonal polynomial constructions in this paper are carried out within a finite-dimensional polynomial space, and as such do not require the existence of moments of all orders.

In the present setting, the orthogonal expansion is truncated at a finite order m; hence, only moments up to order $2m$ are required. For the standardized Student-t distribution, moments of order k exist whenever $\nu > k$. Accordingly, for the fourth-order truncation ($m = 4$) considered in this paper, the condition $\nu > 8$ is sufficient to ensure that the standardized Student-t density serves as a valid finite-order weight function for the subsequent construction.

Proposition 1. *Fix an integer $m \geq 0$. If the degrees of freedom satisfy $\nu > m$, then the standardized Student-t density $t(\cdot;\nu)$ in (1) is an m-order weight function on $(-\infty,\infty)$ in the sense explained above, i.e., properties (1) and (2) of Lemma 1 hold for all $k = 0,1,\ldots,m$. Consequently, all integrals required for the orthogonalization procedure up to degree m are well-defined.*

Proof. We verify the two properties (up to order m) on $(-\infty,\infty)$:

(1) Moments (up to order m). For large $|x|$, the density in (1) behaves as a constant times $|x|^{-(\nu+1)}$. Hence, for any integer $k \geq 0$,

$$\int_R^\infty x^k t(x;\nu)\,\mathrm{d}x < \infty \quad \Longleftrightarrow \quad \int_R^\infty x^{k-(\nu+1)}\,\mathrm{d}x < \infty,$$

which holds precisely when $\nu > k$. Therefore, if $\nu > m$ then all moments of orders $k = 0,1,\ldots,m$ exist and are finite. By symmetry of $t(x;\nu)$ about zero, all odd moments vanish. Moreover, when $k = 2l \leq m$ (so $\nu > 2l$), the even moments admit the closed form

$$\begin{aligned} E\left[X^{2l}\right] &= \int_{-\infty}^{\infty} x^{2l}\, t(x;\nu)\,\mathrm{d}x \\ &= (\nu-2)^l \frac{(2l-1)(2l-3)\cdots 3\cdot 1}{(\nu-2)(\nu-4)\cdots(\nu-2l)} \\ &= (\nu-2)^l \frac{(2l-1)!!}{\prod_{j=1}^{l}(\nu-2j)} = (\nu-2)^l \frac{(2l)!}{2^l\, l!\, \prod_{j=1}^{l}(\nu-2j)}, \qquad (\nu > 2l), \end{aligned} \tag{2}$$

which for $l = 1$ yields $E[X^2] = 1$ (see Xu et al. [25]; for the detailed derivation, see Appendix A.)

(2) Positivity/Non-degeneracy. The density $t(x;\nu)$ is strictly positive and continuous for every $x \in \mathbb{R}$. Let g be continuous with $g \geq 0$ and suppose that $\int_{-\infty}^{\infty} g(x)t(x;\nu)\,\mathrm{d}x = 0$.

If there exists x_0 with $g(x_0) > 0$, continuity gives $\delta > 0$ and $c > 0$ such that $g(x) \geq c$ on $(x_0 - \delta, x_0 + \delta)$. Because $t(x;\nu) > 0$ on that interval,

$$\int_{-\infty}^{\infty} g(x)t(x;\nu)\,\mathrm{d}x \geq c\int_{x_0-\delta}^{x_0+\delta} t(x;\nu)\,\mathrm{d}x > 0,$$

which is a contradiction. Hence, $g \equiv 0$. This argument does not require any restriction on ν.

Combining the two parts shows that for any fixed finite order m, $t(\cdot;\nu)$ satisfies the requirements of Lemma 1 up to order m when $\nu > m$, while the nondegeneracy condition holds unconditionally. □

3. Orthogonal Expansions Based on the Standardized Student-t Distribution

Classical Gram–Charlier (GC) series expansion is one of the earliest approaches that introduces skewness and kurtosis into a symmetric distribution by adding polynomial adjustments to the normal kernel. Because our proposed method is conceptually related to this idea, we briefly present the GC form here for comparison and motivation.

Following León et al. [23], the GC expansion of the normal density is defined as

$$g(x) = \phi(x)\left[1 + \frac{s_t}{3!}(x^3 - 3x) + \frac{k_t - 3}{4!}(x^4 - 6x^2 + 3)\right] = \phi(x)\,\psi(x), \tag{3}$$

where $\phi(x)$ denotes the standard normal density and $\psi(x)$ captures skewness s_t and excess kurtosis $k_t - 3$. Incorporating location and scale gives

$$f(x) = \frac{\phi\big((x-\xi)/\omega\big)\,\psi^2\big((x-\xi)/\omega\big)}{\Gamma_t\,\omega}, \tag{4}$$

$$\Gamma_t = 1 + \frac{s_t^2}{3!} + \frac{(k_t-3)^2}{4!}. \tag{5}$$

For further details, see León et al. [23].

However, GC relies on the Gaussian kernel, and may produce non-positive densities or unstable tail behavior. Motivated by this limitation, the present work constructs a new expansion based on the Student-t distribution, aiming to achieve heavier tails and guaranteed non-negativity after squaring and normalization. The details are developed in the subsequent subsections.

This section develops an orthogonal polynomial expansion for the standardized Student-t density, with the aim of constructing a flexible distribution that allows controlled deviation from symmetry and tail shape. Rather than presenting the framework in a fully abstract form, we derive explicit expansion basis functions under a fixed degrees-of-freedom parameter ν, which will later serve as building blocks for defining the new distributional family introduced in Section 3.2.

We first construct orthogonal polynomials using $t(x;\nu)$ as the weighting kernel (Section 3.1), then derive the corresponding expansion form whose coefficients modulate skewness and kurtosis (Section 3.2). A squaring-and-normalization step ensures non-negativity and proper normalization of the resulting density. We discuss the conditions on ν required for integrability along with the interpretation of the shape parameters (μ_3, μ_4). The formal definition and naming of the resulting distribution is presented after the expanded density is established.

In summary, Section 3.1 builds the orthogonal basis under a given ν, while Section 3.2 applies this basis to derive the explicit expansion form and analyze its parameter-driven shape properties, laying the foundation for defining the proposed t-based distribution in the sequel.

3.1. Orthogonal Polynomials Based on the Student-t Kernel

If $f(x), g(x) \in [a, b]$ and $\rho(x)$ is a weight function on $[a, b]$ such that

$$(f, g) = \int_a^b \rho(x)\, f(x)\, g(x)\, \mathrm{d}x = 0, \tag{6}$$

then f and g are orthogonal with respect to ρ on $[a, b]$ (for further details, refer to [24]).

In the present paper, this notion of orthogonality is used within a finite-dimensional polynomial space. When $\rho(x)$ is an m-order weight function, the inner product (6) is well defined for all polynomials of degree at most m, and orthogonality is understood in this finite-order sense.

Starting from the power basis $\{1, x, \ldots, x^i, \ldots\}$, one constructs orthogonal polynomials $\{\varphi_i\}_{i\geq 0}$ by Gram–Schmidt:

$$\varphi_0(x) = 1, \qquad \varphi_i(x) = x^i - \sum_{j=0}^{i-1} \frac{(x^i, \varphi_j)}{(\varphi_j, \varphi_j)}\, \varphi_j(x), \quad i \geq 1. \tag{7}$$

Because subsequent calculations involve moments up to order eight, we choose the standardized t density, with $\nu = 10$ as the weight on $(-\infty, \infty)$ so that the required moments exist. The choice of $\nu = 10$ is made solely for illustrative purposes; the construction applies to general admissible values of ν. In this setting the inner products in (7) take the form

$$(x^i, \varphi_j) = \int_{-\infty}^{\infty} t(x; \nu)\, x^i\, \varphi_j(x)\, \mathrm{d}x. \tag{8}$$

Applying (7) with this weight yields the first four orthogonal polynomials (for $\nu = 10$):

$$\begin{aligned} &\varphi_0(x) = 1, \quad \varphi_1(x) = x, \quad \varphi_2(x) = x^2 - 1, \\ &\varphi_3(x) = x^3 - 4x, \quad \varphi_4(x) = x^4 - 12x^2 + 8. \end{aligned} \tag{9}$$

These polynomials satisfy the orthogonality relations

$$(\varphi_j, \varphi_k) = \int_{-\infty}^{\infty} t(x; \nu)\, \varphi_j(x)\, \varphi_k(x)\, \mathrm{d}x = \begin{cases} 0, & j \neq k, \\ A_k > 0, & j = k. \end{cases} \tag{10}$$

Lemma 2. *Cramér [26] states that if f is a continuous PDF with corresponding orthogonal polynomials $p_0, p_1, \ldots$, then any other PDF g admits an expansion of the form*

$$g(x) = \sum_{n\geq 0} b_n\, p_n(x)\, f(x) \tag{11}$$

provided the polynomials are orthonormal with respect to f, i.e.,

$$\int_{-\infty}^{\infty} p_m(x) p_n(x) f(x)\, \mathrm{d}x = \begin{cases} 1, & m = n, \\ 0, & m \neq n. \end{cases} \tag{12}$$

Multiplying (11) by p_n and integrating termwise then yields

$$b_n = \int_{-\infty}^{\infty} p_n(x)\, g(x)\, \mathrm{d}x. \tag{13}$$

Applying this result with $f = t(x;\nu)$ and $p_n = \varphi_n$ gives the orthogonal expansion of any PDF g relative to the t-weight:

$$g(x) = \sum_{r\geq 0} c_r\, \varphi_r(x)\, t(x;\nu), \tag{14}$$

where the expansion coefficients are obtained by the inner product

$$c_r = \frac{1}{A_r}\int_{-\infty}^{\infty} \varphi_r(x)\, g(x)\, \mathrm{d}x. \tag{15}$$

Expressing c_r in terms of the raw moments $\mu_k = \int x^k g(x)\,\mathrm{d}x$ yields

$$\begin{aligned} &c_0 = 1, && c_1 = \mu_1,\\ &c_2 = \tfrac{1}{3}(\mu_2 - 1), && c_3 = \tfrac{1}{24}(\mu_3 - 4\mu_1),\\ &c_4 = \tfrac{1}{672}(\mu_4 - 12\mu_2 + 8). \end{aligned}$$

Therefore, truncating the series at fourth order gives the practical approximation

$$\begin{aligned} g(x) = t(x;\nu) &+ \mu_1\varphi_1(x)t(x;\nu) + \tfrac{1}{3}(\mu_2 - 1)\varphi_2(x)t(x;\nu)\\ &+ \tfrac{1}{24}(\mu_3 - 4\mu_1)\varphi_3(x)t(x;\nu) + \tfrac{1}{672}(\mu_4 - 12\mu_2 + 8)\varphi_4(x)t(x;\nu). \end{aligned} \tag{16}$$

For a standardized variable ($\mathbb{E}[X] = 0$, $\mathbb{E}[X^2] = 1$), we have $c_0 = 1$ and $c_1 = c_2 = 0$; hence, the truncated form simplifies to

$$g(x) = \left[1 + \tfrac{1}{24}\mu_3\, \varphi_3(x) + \tfrac{1}{672}(\mu_4 - 4)\, \varphi_4(x)\right] t(x;\nu), \tag{17}$$

with moment constraints

$$\int_{-\infty}^{\infty} x^k g(x)\,\mathrm{d}x = \begin{cases} 0, & k = 1,\\ 1, & k = 2,\\ \mu_3, & k = 3,\\ \mu_4, & k = 4. \end{cases} \tag{18}$$

Thus, the unknown PDF $g(x)$ is approximated by the known baseline $t(x;\nu)$. Although the expansion is in principle infinite, truncation at the fourth order is a standard practical compromise that retains direct interpretability through μ_3 and μ_4 while keeping the approximation compact. This parsimonious parameterization is particularly convenient in empirical finance, where returns commonly display skewness and excess kurtosis. At the same time, truncation introduces approximation error, and for some parameter combinations may lead to regions where the right-hand side becomes negative; these issues motivate our subsequent discussion of admissible parameter regions and positivity-preserving strategies.

3.2. General Form of the Student-t–Weighted Expansion and Its Dependence on the Degrees of Freedom

To study how the expansion depends on the t-baseline, consider a general degrees-of-freedom parameter ν. The first four orthogonal polynomials are

$$\begin{aligned}
&\varphi_0(x) = 1, \quad \varphi_1(x) = x, \quad \varphi_2(x) = x^2 - 1,\\
&\varphi_3(x) = x^3 - \frac{3(\nu-2)}{\nu-4}\,x,\\
&\varphi_4(x) = x^4 - \frac{6(\nu-2)}{\nu-6}\,x^2 + \frac{3(\nu-2)^2}{(\nu-4)(\nu-6)}.
\end{aligned} \tag{19}$$

Their squared norms are

$$\begin{aligned}
&A_0 = (\varphi_0, \varphi_0) = 1, \qquad A_1 = (\varphi_1, \varphi_1) = 1,\\
&A_2 = (\varphi_2, \varphi_2) = \frac{2(\nu-1)}{\nu-4},\\
&A_3 = (\varphi_3, \varphi_3) = \frac{6(\nu-1)(\nu-2)^2}{(\nu-4)^2(\nu-6)},\\
&A_4 = (\varphi_4, \varphi_4) = \frac{24(\nu-1)(\nu-2)^3(\nu-3)}{(\nu-4)^2(\nu-6)^2(\nu-8)}.
\end{aligned} \tag{20}$$

It is convenient to collect the ν-dependent scaling factors into

$$\alpha_3 = \frac{(\nu-4)^2(\nu-6)}{6(\nu-1)(\nu-2)^2}, \quad \alpha_4 = \frac{(\nu-4)^2(\nu-6)^2(\nu-8)}{24(\nu-1)(\nu-2)^3(\nu-3)}, \quad b_v = \frac{3(\nu-2)}{\nu-4}$$

so that for a standardized g the truncated expansion reads

$$g(x) = \Big[1 + \alpha_3\,\mu_3\,\varphi_3(x) + \alpha_4\big(\mu_4 - b_v\big)\varphi_4(x)\Big]\,t(x;\nu) = \psi(x)\,t(x;\nu), \tag{21}$$

where we set

$$\psi(x) = 1 + \alpha_3\mu_3\,\varphi_3(x) + \alpha_4\big(\mu_4 - b_v\big)\varphi_4(x).$$

Note that the linear form in (21) may attain negative values for some parameter combinations; thus, in its original form $g(x)$ is not a valid PDF. Following the suggestion from León et al. [23], we modify $g(x)$ by squaring the polynomial factor and renormalizing to guarantee a non-negative density. We then write the normalized density in abbreviated form as

$$f\big(x;\mu_3,\mu_4,\nu\big) = \frac{\psi(x)^2\,t(x;\nu)}{\mathcal{Z}(\mu_3,\mu_4,\nu)} \tag{22}$$

with the normalizing constant

$$\mathcal{Z}(\mu_3,\mu_4,\nu) = \int_{-\infty}^{\infty} \psi(x)^2\,t(x;\nu)\,\mathrm{d}x. \tag{23}$$

Using the orthogonality of $\{\varphi_r\}$ under the weight $t(x;\nu)$ and squared norms A_3, A_4 in (20), the integral simplifies to

$$\mathcal{Z} = 1 + (\alpha_3\mu_3)^2 A_3 + \big(\alpha_4(\mu_4 - b_v)\big)^2 A_4,$$

meaning that an explicit form of the normalized density is

$$f\big(x;\mu_3,\mu_4,\nu\big) = \frac{\big(1 + \alpha_3\mu_3\varphi_3(x) + \alpha_4(\mu_4 - b_v)\varphi_4(x)\big)^2\,t(x;\nu)}{1 + (\alpha_3\mu_3)^2 A_3 + \big(\alpha_4(\mu_4 - b_v)\big)^2 A_4}. \tag{24}$$

We refer to the family $\{f(x;\mu_3,\mu_4,\nu)\}$ as the Skew–Kurtotic t Expansion (SKTE) distribution in its standardized form. This construction expands the standardized Student-t density by means of orthogonal polynomials, introducing explicit shape control through the parameters μ_3 and μ_4 which regulate skewness and kurtosis, respectively. The baseline

heavy-tailed behavior of the t distribution is preserved, while the polynomial adjustment captures asymmetry and excess peakness. A squaring-and-normalization step guarantees that the resulting function is a valid probability density. Appendix B presents a rigorous proof of the normalization and validity of the proposed standardized SKTE density.

To obtain a flexible family suitable for statistical modeling and empirical applications, we further introduce location and scale parameters. The full Skew–Kurtotic t Expansion (SKTE) density is defined as

$$f_{\mathrm{SKTE}}(x;\nu,\mu_3,\mu_4,\xi,\omega) = \frac{1}{\omega} f\left(\frac{x-\xi}{\omega};\mu_3,\mu_4,\nu\right), \qquad \xi \in \mathbb{R},\ \omega > 0, \tag{25}$$

where $f(\cdot;\mu_3,\mu_4,\nu)$ denotes the standardized SKTE density given in (24).

Equation (25) defines the full SKTE family used in subsequent parameter estimation and empirical analysis, while (24) corresponds to its standardized form.

Although μ_3 and μ_4 originate from the cubic and quartic expansion terms, their meaning after the squaring-and-normalization step differs from that of the classical standardized skewness and kurtosis. Appendix C shows that the third and fourth moments of the resulting density become nonlinear functions of μ_3 and μ_4, denoted as $m_3(\mu_3,\mu_4,\nu)$ and $m_4(\mu_3,\mu_4,\nu)$, rather than being equal to μ_3 and μ_4 directly. Therefore, μ_3 and μ_4 should be interpreted as shape-controlling coefficients; increasing μ_3 shifts mass asymmetrically and mainly affects the third moment, while increasing μ_4 amplifies peakness and tail thickness and primarily drives the fourth moment. The mapping between (μ_3,μ_4) and the resulting moments is monotonic in typical ranges (see Appendix C), meaning that they retain clear interpretability as skewness and kurtosis controllers even though they are no longer identical to the raw moments.

Given that the SKTE density involves polynomial expansions together with a squaring-and-normalization procedure, its algebraic form is considerably more complicated than that of standard parametric models such as the Gaussian or Student-t distribution, which inevitably introduces additional computational burden in practice. Likelihood evaluation requires computing a finite number of orthogonal polynomial terms and handling the normalization constant derived from the squared expansion, consequently increasing the per-iteration cost during parameter estimation. Moreover, the nonlinear structure of the model leads to a more intricate likelihood surface, making the optimization process more sensitive to initialization and regularization strategies. Therefore, appropriate optimization schemes may be needed to achieve stable convergence. Nevertheless, the model remains computationally tractable for typical sample sizes, and the enhanced flexibility in capturing skewness and heavy tails may justify the extra computational cost.

The fourth-order correction in the proposed SKTE model requires $\nu > 8$ to ensure that the squared polynomial is integrable with respect to the t-distributed tails, thereby guaranteeing the existence of the normalizing constant and a proper non-negative probability density function. Although the parameter ν originates from the Student-t kernel, it no longer coincides with the conventional notion of degrees of freedom. In the standard t-distribution, ν directly determines tail thickness and the existence of moments. In contrast, within the SKTE framework ν serves as a structural or tail-regularization parameter that governs the decay rate of the baseline kernel and ensures the integrability and regularity of the squared polynomial terms arising from the orthogonal expansion. Accordingly, the admissible condition $\nu > 8$ guarantees proper normalization of the expanded density rather than the existence of higher-order moments.

From a comparative perspective, the role of ν in SKTE differs fundamentally from that in the classical Student-t distribution. While the degrees of freedom parameter in the classical setting directly controls the tail index and can be interpreted as a measure of tail

thickness, the parameter ν in SKTE primarily determines the tail regime of the underlying kernel and provides structural validity for the squared-and-normalized expansion. As a consequence, although the estimated values of ν in the SKTE model may be of a comparable order of magnitude to those obtained from fitting a standard t-distribution to the same data, the two parameters are not directly comparable in interpretation.

3.3. Truncation Accuracy

To assess the approximation error from truncating the orthogonal expansion at fourth order, we use the standardized Student-t baseline $t(x;\nu)$ with $\nu = 14$. The fourth-order truncated density $f_4(x)$ is defined in Equation (21). As a reference, we employ the sixth-order expansion $f_6(x)$, for which the construction using the fifth- and sixth-order orthogonal polynomials φ_5 and φ_6 is given in Appendix D. The coefficients μ_k for $k = 5, 6$ are used in f_6 to represent plausible higher-order contributions absent in f_4; hence, f_6 serves as a controlled proxy for a higher-order approximation and allows us to evaluate truncation effects empirically.

Two representative parameter regimes are examined:

- Moderate regime: $\mu_3 = 0.5, \mu_4 = 4.5, \mu_5 = 0.1, \mu_6 = 0.2$, reflecting typical empirical skewness and kurtosis with small higher-order contributions.
- Large regime: $\mu_3 = 1.0, \mu_4 = 6.0, \mu_5 = 3.0, \mu_6 = 4.0$, representing pronounced skewness and peakness with substantial higher-order effects.

Performance is measured by the following:

- Integrated Absolute Difference (IAD): $\mathrm{IAD} = \int_{-\infty}^{\infty} |f_6(x) - f_4(x)|\, \mathrm{d}x$ (global bias).
- Supremum norm: $\|f_6 - f_4\|_\infty = \sup_x |f_6(x) - f_4(x)|$ (local maximal deviation).
- Tail-mass differences over $|x| > c$ for $c \in \{3, 4, 5\}$.
- Quantile-location differences for selected quantiles (1%, 5%, 95%, 99%).

3.3.1. Numerical Results

Numerical integrals and Cumulative Distribution Function (CDF) inversions were computed on a dense grid $x \in [-80, 80]$ using the trapezoidal rule; CDF arrays were enforced to be monotone prior to inversion. Denoting $\mathrm{diff} = \mathrm{value}_{m_6} - \mathrm{value}_{m_4}$, the results in Tables 1 and 2 indicate that the fourth-order truncation provides a satisfactory approximation for the bulk of the distribution and for moderately extreme quantiles under moderate levels of skewness and kurtosis. For more pronounced skewness/kurtosis and for very extreme tail probabilities (e.g., the 1% lower quantile), higher-order terms become increasingly important, reflecting the inherent numerical sensitivity of truncated expansions in the far tails.

Table 1. Truncation errors measured by the Integrated Absolute Difference (IAD), sup-norm error, and left/right tail probability differences, comparing fourth- and sixth-order truncations under different scenarios.

Scen.	**IAD**	**Sup**	$\lvert x\rvert > 3$			$\lvert x\rvert > 4$			$\lvert x\rvert > 5$		
			m_6	m_4	**diff**	m_6	m_4	**diff**	m_6	m_4	**diff**
Mod.	0.139	0.055	0.099	0.068	0.031	0.047	0.032	0.015	0.025	0.018	0.007
Large	0.191	0.065	0.222	0.134	0.088	0.119	0.103	0.016	0.041	0.064	−0.024

Note. Scen. = scenario; Mod. = moderate. Sup = sup-norm. diff = $m_6 - m_4$. All values are rounded to three decimals.

Table 2. Quantile comparisons between the sixth- and fourth-order truncations, including $q_{\alpha,6}$, $q_{\alpha,4}$, and their difference $q_{\alpha,6} - q_{\alpha,4}$, all over $x \in [-80, 80]$, illustrating truncation effects on bulk and tail quantiles.

Scenario	Quantile	$q_{\alpha,6}$	$q_{\alpha,4}$	diff
Moderate	0.01	-13.261 †	-2.174	-11.086 †
	0.05	-1.728	-1.563	-0.165
	0.95	2.063	1.912	0.151
	0.99	3.230	3.554	-0.324
Large	0.01	-9.515 †	-2.814	-6.702 †
	0.05	-1.624	-1.584	-0.040
	0.95	3.045	2.795	0.250
	0.99	9.750	5.337	4.413

Note. $q_{\alpha,k}$ denotes the α-quantile from the kth-order truncated density ($k \in \{4, 6\}$); the last column reports the difference diff = $q_{\alpha,6} - q_{\alpha,4}$. † Extreme lower quantiles remain numerically sensitive under the current grid resolution.

3.3.2. Theoretical Error Bound

Let $f_\infty(x)$ denote the full (infinite-order) orthogonal expansion. For the fourth-order truncated density $f_4(x)$, the truncation error can be bounded by

$$\|f_4 - f_\infty\|_1 \leq \sum_{k=5}^{\infty} |\mu_k| \, \|\varphi_k\|_1,$$

where μ_k are expansion coefficients and φ_k the orthogonal polynomials. Although exact coefficients beyond $k = 6$ are unknown in practice, the magnitude of μ_5 and μ_6 suggests that the remainder is small for moderate skewness and kurtosis, providing a conservative theoretical bound.

3.3.3. Guideline for Choosing Truncation Order

A practical criterion for selecting the expansion order m is to control either (i) the Integrated Absolute Difference (IAD) or (ii) extreme quantile deviations relative to a pre-specified tolerance ϵ. Formally, one may choose

$$m^* = \min\left\{ m : \begin{array}{l} \mathrm{IAD}_m = \int |f_m(x) - f_{m-1}(x)| \, dx < \epsilon, \\ \text{or} \quad \max_\alpha |q_{\alpha,m} - q_{\alpha,m-1}| < \epsilon_q \end{array} \right\}.$$

This provides a simple adaptive procedure that balances approximation accuracy and model complexity.

3.3.4. Remark

The theoretical bound and the order-selection guideline above are presented to clarify the mechanism and magnitude of truncation effects in the orthogonal expansion. Because the higher-order coefficients μ_k ($k \geq 5$) are not identifiable from data, the bound is not evaluated numerically; instead, the empirical comparison between the fourth- and sixth-order expansions provides a practical validation that the remaining truncation error is small within the parameter regimes relevant to our applications.

It should be noted that the truncation error analysis presented above is necessarily conducted under a limited set of parameter configurations. In particular, the conclusion regarding the practical sufficiency of the fourth-order truncation is mainly intended for moderate values of the shape parameters, corresponding to distributions with mild to moderate skewness and tail heaviness. Under such conditions, the comparison with a

sixth-order expansion serves as a reasonable auxiliary benchmark for assessing the accuracy of the truncated representation.

For more extreme distributional shapes, such as cases with very high skewness or extremely heavy tails, higher-order terms may be required to achieve a comparable level of approximation accuracy. This limitation is common to truncated orthogonal expansion methods, and does not undermine the validity of the proposed SKTE framework; rather, it highlights the tradeoff between model flexibility and analytical tractability, and suggests that the fourth-order specification should be viewed as a parsimonious yet effective approximation within a practically relevant parameter range.

4. Empirical Comparison of Distributional Models Using Historical Financial Returns

4.1. Data Description and Preliminary Analysis

The empirical analysis employs daily closing prices obtained from Yahoo Finance [27] (accessed on 10 September 2025) for four assets: the Hang Seng Index (HSI, ticker: ^HSI), the S&P 500 Index (ticker: ^GSPC), the front-month natural gas futures contract (ticker: ^NG=F), and the EUR/USD exchange rate (ticker: ^EURUSD=X). To ensure comparability across different trading calendars, we restrict the sample to overlapping trading days from 2 January 2020 to 27 June 2025. This restriction yields 1311 daily price observations for each asset, corresponding to 1310 daily log-return values.

This sample period spans several structurally important market phases, including the COVID-19 crisis, the post-pandemic recovery, the 2021–2022 commodity price shocks, and the subsequent monetary tightening cycles. These episodes provide a rich environment characterized by elevated volatility, asymmetry, and heavy-tailed behavior, making the dataset particularly suitable for evaluating the performance of alternative distributional models under realistic stress conditions.

Our selection of these four assets is guided by statistical considerations aimed at ensuring robustness, comparability, and generalizability of the empirical findings. From a distributional modeling perspective, it is desirable to include return series that differ in volatility, skewness, and tail thickness to ensure that model performance can be evaluated across heterogeneous data-generating mechanisms. Equity indices from Asia (HSI) and the United States (S&P 500), an energy commodity (natural gas futures), and a major currency pair (EUR/USD) jointly provide a balanced representation of markets with distinct liquidity conditions, trading frictions, and shock transmission channels. Such diversity helps to mitigate sample-specific bias and allows for stress-testing of distributional models over return processes that exhibit varying degrees of serial dependence, volatility clustering, asymmetry, and extreme observations. Furthermore, restricting all assets to overlapping trading days ensures temporal alignment, prevents asynchronous sampling bias, and supports meaningful cross-asset comparisons. This statistically grounded selection strategy enhances the reliability of tail inference and ensures that subsequent model evaluation is not driven by idiosyncratic features of a single market.

Building on this statistically grounded selection, we next construct daily log-return series for the four assets and examine their basic distributional features. Daily log-returns r_t are computed as

$$r_t = \ln\left(\frac{P_t}{P_{t-1}}\right),$$

where P_t denotes the closing price on trading day t. Table 3 reports descriptive statistics for each return series, including the mean, standard deviation (Std.), selected percentiles (25th, median, 75th), minimum (Min), maximum (Max), skewness, and kurtosis. These statistics provide initial insights into cross-asset differences in central tendency, volatility, and tail

behavior, motivating the empirical comparison of competing distributional models in the subsequent sections.

Table 3. Descriptive statistics of daily log-returns on common trading days over the period 2 January 2020–27 June 2025, highlighting asymmetry and excess kurtosis in financial returns.

Statistic	HSI	S&P 500	NG	EUR/USD
Sample size		1310		
Mean	−0.0123	0.0488	0.0432	0.0031
Std. dev.	1.6398	1.3912	4.7845	0.5055
Min	−14.1833	−12.7652	−30.0480	−2.8144
25th percentile	−0.9375	−0.5403	−2.7316	−0.2881
Median	−0.0226	0.0911	0.0412	−0.0031
75th percentile	0.8479	0.7346	2.7423	0.3005
Max	8.6928	9.0895	38.1727	2.7537
Skewness	−0.3485	−0.6167	0.2375	0.0872
Kurtosis	9.5406	16.4939	8.1185	5.4467

Table 3 summarizes the key statistical properties of daily log-returns for the four assets. Among them, the natural gas futures (NG) exhibit the highest volatility, reflecting the pronounced price fluctuations that are typical of energy commodities, while the EUR/USD exchange rate displays the lowest volatility across the sample. The two equity indices, HSI and S&P 500, show moderate levels of volatility accompanied by negative skewness and pronounced kurtosis, indicating asymmetric and heavy-tailed return distributions. In contrast, NG returns are slightly positively skewed, whereas EUR/USD returns appear approximately symmetric.

These preliminary findings indicate that the normality assumption is insufficient to capture the empirical distributional features of asset returns, particularly in the tails. The presence of both skewness and excess kurtosis highlights the need for more flexible models that can accommodate asymmetry and heavy tails. Such models are expected to yield a more accurate representation of tail risk and return dynamics, which is essential for subsequent applications such as value-at-risk estimation, option pricing, and portfolio risk assessment.

4.2. Models and Estimation

Preliminary examination of the return series reveals pronounced skewness and heavy tails, indicating that Gaussian assumptions may be insufficient. To model these non-Gaussian characteristics, we focus on two flexible alternatives and estimate them in a unified location–scale framework with parameters (ξ, ω). Specifically, we consider the classical Gram–Charlier (GC) expansion of the normal density as a benchmark and contrast it with the proposed Skew–Kurtotic t Expansion (SKTE).

Both models belong to the class of expansion-based distributional approaches, in which departures from symmetry and Gaussianity are captured through higher-order polynomial corrections. While the GC expansion incorporates such adjustments on top of a Gaussian kernel, SKTE extends this principle to a Student-t basis, thereby allowing for simultaneous control over skewness, kurtosis, and tail heaviness within a unified framework. In empirical implementation, the GC model is applied in its standard fourth-order truncated form (Section 3, Equation (3)), whereas SKTE follows the formulation given in Equation (24).

From a methodological perspective, the empirical comparison focuses primarily on GC as the natural benchmark for SKTE. Because both models share the same expansion-based structure, this comparison provides a direct and transparent assessment of the effect on stability and tail behavior when replacing the Gaussian kernel with a heavy-tailed

Student-t kernel. Alternative models frequently used in financial applications, such as Azzalini-type skew-t distributions as well as GED or NIG models, are constructed under different parametric paradigms and do not rely on orthogonal expansion mechanisms. As a result, their parameters are not directly comparable to the expansion coefficients in SKTE, and including them would require a broader comparative study across heterogeneous model classes, which lies beyond the primary scope of the present paper.

Nevertheless, the empirical evidence presented below demonstrates that even when compared against its closest methodological counterpart, the classical GC expansion, the SKTE model achieves substantial improvements in terms of tail stability and goodness of fit. This finding supports the central contribution of the paper, namely, that incorporating a heavy-tailed kernel into an expansion-based framework provides a principled and effective way to model skewed and heavy-tailed financial return distributions.

Parameter estimation is carried out by Maximum Likelihood Estimation (MLE) on the original data scale using a two-stage numerical optimization procedure. The algorithm proceeds as follows:

1. Global initialization: A population-based Differential Evolution (DE) algorithm is first applied over bounded parameter spaces to explore the likelihood surface and obtain robust initial parameter values. The DE algorithm is implemented with a maximum of 40 iterations and a population size of 15. To ensure full reproducibility, random seeds are fixed at this stage.
2. Local refinement: The parameter vector obtained from the global stage is then used as the starting point for a local optimization based on a bound-constrained quasi-Newton method (L-BFGS-B), which minimizes the negative log-likelihood function.
3. Constraint handling and numerical stability: Parameter constraints are enforced throughout the optimization process, including positivity of scale parameters and lower-bound restrictions on shape parameters. Any infeasible parameter values or numerically invalid likelihood evaluations are penalized by assigning an infinite objective value, thereby preventing the optimizer from entering inadmissible regions.
4. Convergence and inference: Convergence of the local optimizer is determined by the standard stopping criteria of the L-BFGS-B routine based on improvements in the objective function and the magnitude of projected gradients under bound constraints. Upon convergence, standard errors are computed from the observed information matrix evaluated at the optimum.

4.3. Quantitative Comparison (NLL/AIC/BIC)

To evaluate model performance, we compute several goodness-of-fit criteria, including the Negative Log-Likelihood (NLL), Akaike Information Criterion (AIC), and Bayesian Information Criterion (BIC). Lower values of these metrics indicate a better tradeoff between model fit and parsimony.

Table 4 reports the estimated parameters together with the NLL, AIC, and BIC for the four assets. For clarity, all NLL, AIC, and BIC values are rounded to the nearest integer. The results allow a direct comparison between the GC expansion and the proposed SKTE distribution in terms of their empirical adequacy and parameter interpretability. It should be noted that the estimated values of μ_3 and μ_4 reported in Table 4 should be interpreted as shape-control coefficients rather than as moment-based skewness and kurtosis. In particular, their magnitudes indicate the extent to which asymmetry and tail thickness are adjusted relative to the underlying t kernel, and should not be directly compared with classical moment estimates.

Table 4. Estimated parameters and goodness-of-fit statistics (NLL, AIC, and BIC) for the SKTE and Gram–Charlier (GC) distributions across four assets, facilitating a direct comparison of empirical fit and parameter behavior across models.

	HSI		**S&P 500**		**NG**		**EUR/USD**	
	SKTE	**GC**	**SKTE**	**GC**	**SKTE**	**GC**	**SKTE**	**GC**
μ_3	0.1084	20	−0.5432	−19.3494	−0.0841	0.0117	−0.0046	−18.5804
μ_4	7.3550	41.0086	4.2947	38.1612	3.6118	3.1924	8.1178	38.7026
ν	8.2229	–	12.2911	–	9.6080	–	8.1237	–
ξ	0.0652	−8.0931	−0.0138	7.1911	0.1496	−1.7732	−0.0186	2.7042
ω	1.4165	2.4453	0.9735	2.1723	4.0394	6.0965	0.4407	0.8119
NLL	2439	3021	2080	2752	3853	4013	926	1547
AIC	4888	6051	4170	5513	7717	8035	1863	3103
BIC	4914	6071	4196	5534	7742	8056	1889	3123

Note: NLL, AIC, and BIC values are rounded to the nearest integer.

The estimation results in Table 4 show consistent evidence that the proposed SKTE distribution provides a superior fit relative to the GC expansion across all four assets. Specifically, SKTE achieves substantially lower values of Negative Log-Likelihood (NLL), Akaike Information Criterion (AIC), and Bayesian Information Criterion (BIC), indicating both higher likelihood and greater model parsimony.

It is worth emphasizing that the parameter ν in the SKTE model plays a role that differs from the classical degrees of freedom in the Student-t distribution. In the proposed framework, ν primarily serves a structural purpose; it determines the tail behavior of the baseline kernel used in the orthogonal expansion, and ensures the integrability and regularity conditions required for the squared-and-normalized density construction. As such, ν acts as a tail-regularization parameter at the kernel level rather than as a direct measure of tail thickness of the resulting distribution. From an empirical perspective, the estimated values of ν characterize the tail regime of the underlying t kernel rather than the tail thickness of the final SKTE density itself. For the equity indices (HSI and S&P 500), ν typically ranges between 8 and 12, indicating a moderately heavy-tailed baseline kernel.

We note that although the estimated degrees of freedom ν for some assets are close to the theoretical lower bound required by the fourth-order truncation, this condition represents a sufficient moment-existence criterion rather than a numerical stability threshold. As long as ν exceeds this bound, the finite-order orthogonal expansion remains well defined and the resulting likelihood-based estimation is numerically stable.

It should be noted that the parameter estimates reported in Table 4 are obtained via maximum likelihood based on the truncated SKTE density, and do not rely on the closed-form moment expressions derived in Appendix C. Those moment formulas are included for interpretational purposes only.

The associated shape-control parameter μ_3 captures the negative asymmetry of the S&P 500 returns and the mild positive skewness of HSI, which is consistent with the observed sample moments. For the natural gas futures (NG), a smaller value of ν implies that a heavier-tailed kernel is required to accommodate the higher volatility and extreme observations commonly observed in energy markets. In contrast, the EUR/USD series is characterized by a relatively small scale parameter ω, suggesting more stable daily fluctuations compared to equity and commodity returns. Overall, these results illustrate that ν governs the baseline tail behavior, while the final distributional shape is jointly determined by ν and the expansion-based shape parameters.

It is worth noting that the classical Gram–Charlier (GC) expansion yields extremely large estimates of the skewness and kurtosis parameters, such as $\mu_3 \approx -19$ and $\mu_4 \approx 38$

reported in Table 4. This behavior reflects a well-known tail mismatch compensation effect. Because the GC model relies on a Gaussian kernel with light tails, the higher-order polynomial coefficients are forced to take unusually large values in order to compensate for the inability of the kernel to capture the heavy-tailed empirical distribution. As a result, the estimated skewness and kurtosis parameters may become inflated, signaling numerical instability rather than genuine distributional features. This phenomenon highlights a fundamental limitation of the GC expansion in heavy-tailed settings and provides further empirical support for the proposed SKTE model, which incorporates tail heaviness directly at the kernel level.

Overall, these results confirm that the SKTE model flexibly adapts to different market conditions, offering a more accurate characterization of skewness and tail behavior than the polynomial-based GC expansion.

Beyond statistical fit, the empirical results in Table 4 also carry clear economic and statistical implications. From a statistical perspective, the uniformly lower NLL, AIC, and BIC values obtained by the SKTE model across all four assets indicate that allowing for flexible and kernel-based control of skewness and tail thickness leads to a more faithful representation of the underlying return distributions. Importantly, the improvement is consistent across assets and evaluation criteria, suggesting that the gains are systematic rather than asset-specific or driven by overfitting.

From an economic perspective, the estimated parameters imply that financial assets exhibit pronounced asymmetry and heterogeneous tail risk that cannot be adequately captured by moment-based expansions. The SKTE model accommodates these features through smooth and stable shape adjustments relative to a heavy-tailed t kernel, which is particularly relevant for modeling downside risk and extreme market movements. In contrast, the Gram–Charlier expansion attempts to compensate for tail mis-specification through inflated higher-order coefficients, resulting in unstable parameter estimates and weaker economic interpretability.

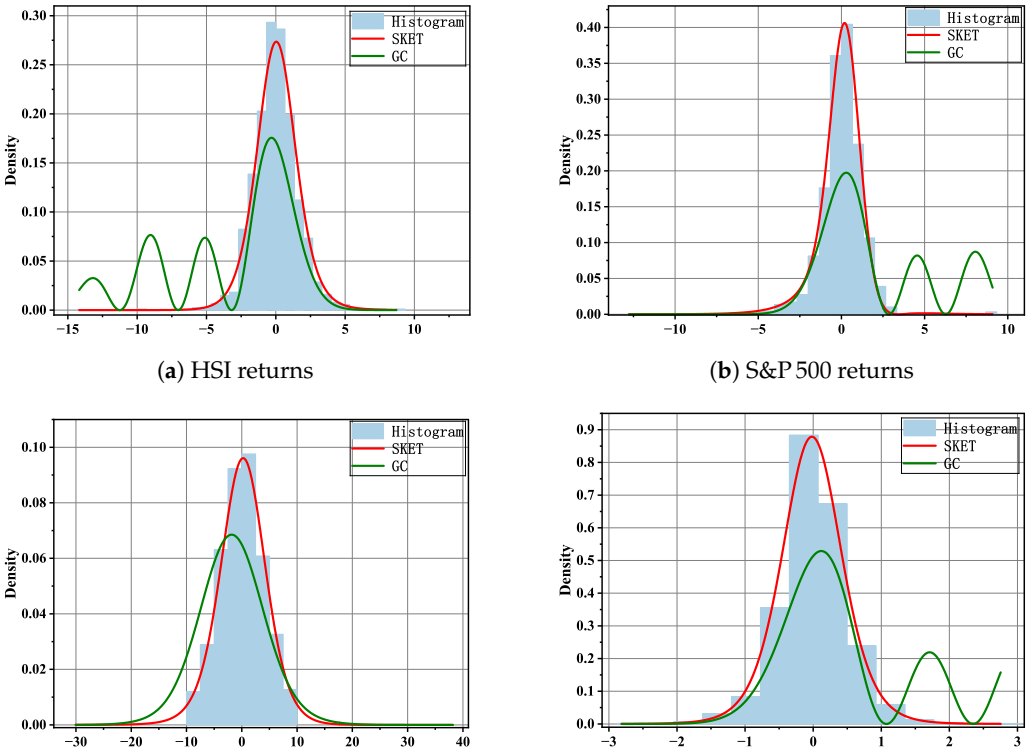
Our comparison of goodness-of-fit measures across models further reinforces this distinction. While lower AIC and BIC values indicate superior statistical performance, they also imply that the SKTE model achieves this improvement without excessive parameter inflation, thereby offering a more parsimonious and economically meaningful description of return dynamics. As a result, the SKTE framework provides not only better in-sample fit but also a more reliable basis for subsequent risk assessment and financial decision-making.

To further illustrate the relative performance of the competing models, we visualize the fitted densities and corresponding quantile-quantile (Q–Q) plots. Specifically, for each asset, the empirical histogram of daily log-returns is overlaid with the estimated probability density functions of the SKTE and GC models. The Q–Q plots compare empirical quantiles with those implied by each fitted distribution, providing an additional diagnostic for tail behavior and overall goodness of fit.

4.4. Visual Diagnostics (Densities and Q–Q)

Figure 1a–d show the empirical return histograms together with the fitted SKTE and GC density curves. Across all markets, the SKTE density (red) follows the empirical distribution closely, capturing both the peak around the center and the heavy-tailed behavior. In contrast, the GC curve (green) exhibits noticeable oscillations in the tails and tends to underestimate extreme return probability mass. This underestimation is especially visible in the HSI and S&P 500 series, where the GC density drops too quickly in both directions, while SKTE maintains heavier tails that align better with the data. For the NG market, a series that is characterized by particularly large price fluctuations, SKTE adapts to the thicker tails effectively, whereas GC again shows tail distortion and overly smooth curvature. Even

for the relatively mild EUR/USD returns, SKTE exhibits a more accurate central peak and balanced decay rate, whereas GC produces visible wiggles and assigns insufficient mass to tail regions.



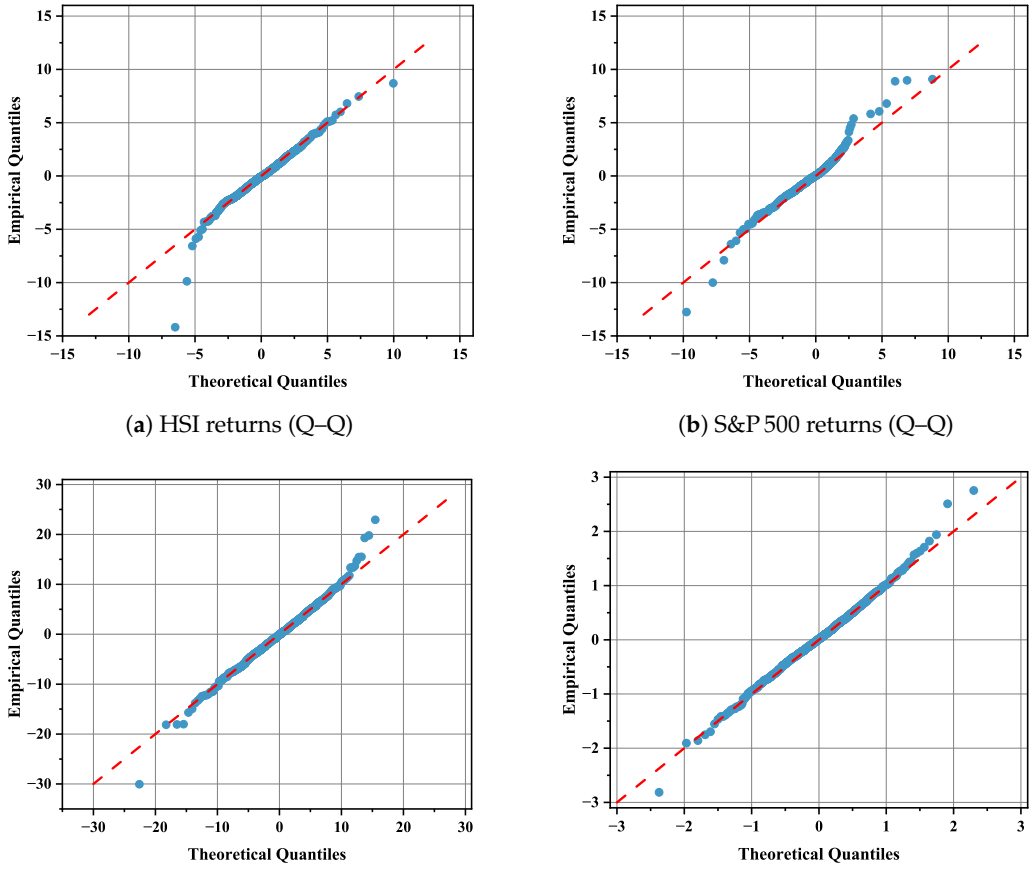
(**a**) HSI returns (**b**) S&P 500 returns

(**c**) NG returns (**d**) EUR/USD returns

Figure 1. Empirical return distributions (histograms) together with fitted density curves under the SKTE and Gram–Charlier (GC) models for four assets: (**a**) HSI, (**b**) S&P 500, (**c**) NG, and (**d**) EUR/USD. The comparison illustrates differences in central fit and tail behavior between the two models.

Overall, the comparison suggests that SKTE provides a more stable and realistic fit across diverse assets. Its ability to capture tail thickness and asymmetry without generating oscillatory artifacts offers a substantial improvement over the GC expansion, underscoring the benefit of using a t-kernel framework with explicit skewness-kurtosis control.

Figure 2a–d shows Q–Q plots comparing empirical returns with the fitted SKTE quantiles. The points cluster closely around the 45-degree line, demonstrating that SKTE provides an accurate approximation to the empirical distribution across the central region. Mild departures appear in the far tails, where extreme price movements occur infrequently but with large magnitude. These observations are characteristic of heavy-tailed financial returns, and do not indicate poor model performance; instead, they highlight the intrinsic difficulty of fitting extreme events with finite-sample information. Despite this, SKTE still tracks the tail area well relative to typical parametric models, confirming its advantage in modeling asymmetric and heavy-tailed behavior. Overall, the Q–Q analysis suggests that the SKTE distribution is well suited for financial return modeling, with deviations arising mainly from rare tail events rather than from structural misfit.



(**a**) HSI returns (Q–Q)

(**b**) S&P 500 returns (Q–Q)

(**c**) NG returns (Q–Q)

(**d**) EUR/USD returns (Q–Q)

Figure 2. Q–Q plots comparing empirical return quantiles with the corresponding theoretical quantiles of the fitted SKTE distributions for four assets: (**a**) HSI, (**b**) S&P 500, (**c**) NG, and (**d**) EUR/USD. In each plot, the dots represent the empirical quantiles, and the dashed line represents the 45-degree reference line.

4.5. Summary of Empirical Findings

Building on the numerical and visual assessments, the SKTE distribution consistently outperforms the GC expansion across all assets in terms of the Negative Log-Likelihood (NLL), Akaike Information Criterion (AIC), and Bayesian Information Criterion (BIC). Its additional degrees-of-freedom parameter ν allows for explicit control over tail thickness, while the estimated skewness and kurtosis adjustments remain moderate and stable. The inclusion of location and scale parameters ensures accurate asset-specific alignment.

In contrast, the GC expansion sometimes yields less stable parameter estimates and exhibits inferior tail representation, particularly for extreme returns. Overall, these findings indicate that SKTE provides a robust and flexible framework for modeling financial returns. It effectively captures asymmetry and heavy tails, which are crucial features for risk measurement, derivative pricing, and portfolio management.

5. Conclusions

This paper develops the Skew–Kurtotic t Expansion (SKTE), a flexible and robust framework for modeling financial asset returns that simultaneously accounts for skewness, excess kurtosis, and heavy tails. By constructing orthogonal polynomials with respect to the standardized Student-t density, the proposed SKTE provides a parsimonious and interpretable parameterization while preserving the essential heavy-tailed characteristics of financial returns. Squaring and normalization ensure that the resulting expansion defines a valid probability density. In addition, truncation accuracy analysis demonstrates that a

fourth-order approximation balances computational efficiency with faithful representation of tail behavior, with higher-order terms contributing negligible improvement.

Empirical analysis using daily returns from the Hang Seng Index, S&P 500, front-month natural gas futures, and the EUR/USD exchange rate shows that SKTE consistently outperforms the classical Gram–Charlier expansion, particularly in capturing extreme movements and adjusting skewness and kurtosis. Maximum likelihood estimation confirms that the model delivers stable parameter estimates while allowing for asset-specific alignment through location and scale parameters. These results highlight SKTE's ability to provide accurate risk quantification and improved modeling of extreme market events, which are critical for value-at-risk computations, derivative pricing, and portfolio risk management.

Several promising directions remain for future study. These include designing fast approximation schemes or gradient-based optimization methods to improve numerical efficiency, developing scalable algorithms for large-sample settings, and exploring sparse or decomposable polynomial bases for high-dimensional extensions. Such developments could further enhance the applicability of SKTE in high-frequency finance, large-scale risk assessment, and multivariate modeling.

Author Contributions: J.Y.: writing—original draft, software, methodology, and conceptualization; Z.Z.: methodology, writing—review and editing, supervision. All authors have read and agreed to the published version of the manuscript.

Funding: This research did not receive any specific grant from funding agencies in the public, commercial, or not-for-profit sectors.

Data Availability Statement: The data used in this study were derived from publicly available stock price data obtained from Yahoo Finance (https://finance.yahoo.com (accessed on 10 September 2025)). The processed data (daily returns) are available from the corresponding author upon reasonable request.

Acknowledgments: The authors are thankful to the editor, co-editor, and referees for their valuable comments, which have significantly enhanced the quality of this article.

Conflicts of Interest: The authors declare that they have no known competing financial interests or personal relationships that could have influenced or appeared to influence the work reported in this paper.

Appendix A. Recursive Derivation of Moments for the Standardized Student-t Distribution

Proof. We start by noting that if $X \sim t(n)$, then $X = \frac{U}{\sqrt{V/n}}$, where $U \sim N(0,1)$, $V \sim \chi^2(n)$, and U is independent of V. Thus, the expectation $E(X^k)$ can be expressed as

$$E(X^k) = n^{k/2} E(U^k) E(V^{-k/2}). \tag{A1}$$

Case 1: k is odd.

For odd k, the expectation $E(U^k) = 0$, because the odd moments of a normal distribution are zero. Therefore, $E(X^k) = 0$ when k is odd.

Case 2: $k = 2l$ is even.

When k is even, i.e., $k = 2l$, the expectation $E(U^k)$ can be computed as

$$\begin{aligned} E\left(U^k\right) &= \frac{2^l}{\sqrt{\pi}}\Gamma\left(l+\frac{1}{2}\right) \\ &= \frac{2^l}{\sqrt{\pi}}\left(l+\frac{1}{2}-1\right)\left(l+\frac{1}{2}-2\right)\cdots\frac{3}{2}\frac{1}{2}\Gamma\left(\frac{1}{2}\right) \\ &= (2l-1)(2l-3)\cdots 3\cdot 1. \end{aligned} \tag{A2}$$

The expectation $E(V^{-k/2})$ is given by

$$\begin{aligned} E\left(V^{-k/2}\right) &= \frac{\Gamma\left(\frac{n-k}{2}\right)}{2^{k/2}\Gamma\left(\frac{n}{2}\right)} = \frac{\Gamma\left(\frac{n}{2}-l\right)}{2^{l}\Gamma\left(\frac{n}{2}\right)} \\ &= \frac{1}{(n-2)(n-4)\cdots[n-2(l-1)](n-2l)}. \end{aligned} \tag{A3}$$

Combining these results, we arrive at the final expression for $E(X^k)$ when k is even:

$$E\left(X^k\right) = n^l \frac{(2l-1)(2l-3)\cdots 3\cdot 1}{(n-2)(n-4)\cdots[n-2(l-1)](n-2l)}. \tag{A4}$$

Now, let $T = \frac{X}{\sqrt{\frac{n}{n-2}}}$, which represents the standardization process. From this, we can obtain a random variable that follows a standard Student-t distribution with mean 0 and variance 1.

Then, according to Equation (A4), when $k = 2l$ is even, the moment of T can be expressed as

$$\begin{aligned} E\left(T^k\right) &= \left(\sqrt{\frac{n-2}{n}}\right)^k E(X^k) \\ &= (n-2)^l \frac{(2l-1)(2l-3)\cdots 3\cdot 1}{(n-2)(n-4)\cdots[n-2(l-1)](n-2l)}. \end{aligned} \tag{A5}$$

Obviously, when k is odd, $E(T^k) = 0$.

The proof is completed. □

Appendix B. Proof that the Standardized Student-t Expansion Defines a Valid Density

In this appendix, we show that the squared-and-normalized construction

$$f(x;\mu_3,\mu_4,\nu) = \frac{\psi(x)^2\, t(x,\nu)}{\mathcal{Z}(\mu_3,\mu_4,\nu)}, \qquad \psi(x) = 1 + \alpha_3\mu_3\,\varphi_3(x) + \alpha_4(\mu_4 - b_\nu)\,\varphi_4(x)$$

with

$$\mathcal{Z}(\mu_3,\mu_4,\nu) = \int_{-\infty}^{\infty} \psi(x)^2\, t(x,\nu)\,\mathrm{d}x$$

indeed defines a probability density under the usual requirement on the degrees of freedom ν. Here, $t(x,\nu)$ denotes the standardized Student-t density with ν degrees of freedom, $\{\varphi_r\}$ are the orthogonal polynomials with respect to $t(x,\nu)$, and $\alpha_3, \alpha_4, b_\nu$ are as in the main text.

Proof. We prove two properties in turn, namely, non-negativity and normalization.

(i) Non-negativity. For every real x, we have $\psi(x)^2 \geq 0$. The standardized Student-t density satisfies $t(x,\nu) > 0$ for all $x \in \mathbb{R}$. Hence, the numerator $\psi(x)^2 t(x,\nu)$ is non-negative for all x; therefore,

$$f(x;\mu_3,\mu_4,\nu) \geq 0 \quad \text{for all } x \in \mathbb{R},$$

provided that the normalizing constant $\mathcal{Z}$ is finite and positive (addressed below). Thus, f is pointwise non-negative.

(ii) Normalization. By the definition of $\mathcal{Z}$,

$$\int_{-\infty}^{\infty} f(x;\mu_3,\mu_4,\nu)\,\mathrm{d}x = \frac{1}{\mathcal{Z}}\int_{-\infty}^{\infty} \psi(x)^2\, t(x,\nu)\,\mathrm{d}x = \frac{\mathcal{Z}}{\mathcal{Z}} = 1,$$

provided $\mathcal{Z} \in (0, \infty)$. Hence, f integrates to one when $\mathcal{Z}$ is well-defined and positive.

(iii) Finiteness and explicit form of $\mathcal{Z}$. Expand $\psi(x)^2$ as follows:

$$\begin{aligned}\psi(x)^2 = 1 &+ 2\alpha_3\mu_3\varphi_3(x) + 2\alpha_4(\mu_4 - b_v)\varphi_4(x) \\ &+ (\alpha_3\mu_3)^2\varphi_3(x)^2 + \big(\alpha_4(\mu_4 - b_v)\big)^2\varphi_4(x)^2 \\ &+ 2\alpha_3\alpha_4\mu_3(\mu_4 - b_v)\varphi_3(x)\varphi_4(x).\end{aligned}$$

Integrating termwise against $t(x, \nu)$ and using the orthogonality of $\{\varphi_r\}$, we have

$$\int \varphi_j(x)t(x,\nu)\,\mathrm{d}x = 0 \quad (j \geq 1), \qquad \int \varphi_j(x)\varphi_k(x)t(x,\nu)\,\mathrm{d}x = 0 \quad (j \neq k).$$

Hence, all linear and cross terms vanish:

$$\mathcal{Z} = \int \psi(x)^2 t(x,\nu)\,\mathrm{d}x = 1 + (\alpha_3\mu_3)^2 A_3 + \big(\alpha_4(\mu_4 - b_v)\big)^2 A_4,$$

where $A_3 = \int \varphi_3(x)^2 t(x,\nu)\,\mathrm{d}x$ and $A_4 = \int \varphi_4(x)^2 t(x,\nu)\,\mathrm{d}x$ are the squared norms given in (20) of the main text. Each term on the right-hand side is non-negative, and the sum is strictly positive unless simultaneously $\mu_3 = \mu_4 - b_v = 0$ (in which case $\mathcal{Z} = 1$); hence, $\mathcal{Z} > 0$.

(iv) Integrability condition on ν. The integrability of the highest-degree term is determined by the tail behavior of $t(x, \nu)$. Because $t(x,\nu) \sim C|x|^{-\nu-1}$ as $|x| \to \infty$ and since $\psi(x)^2$ grows at most like a constant times $|x|^8$ (square of a fourth-degree polynomial), the integrand $\psi(x)^2 t(x,\nu)$ is integrable at infinity provided that

$$\int^{\infty} x^8 x^{-\nu-1}\,\mathrm{d}x < \infty \quad \Longleftrightarrow \quad \nu > 8.$$

Equivalently, the explicit expressions for A_3 and A_4 in (20) show that A_3 is finite for $\nu > 6$ and that A_4 is finite for $\nu > 8$. Consequently, the construction above yields a finite $\mathcal{Z}$ (and hence a bona fide PDF) provided $\nu > 8$. If $\nu \leq 8$, then one must either lower the polynomial order or choose a different baseline density so that the required moments exist.

Conclusions. For any real μ_3, μ_4 and any degrees-of-freedom parameter $\nu > 8$, the function $f(x; \mu_3, \mu_4, \nu)$ defined above is non-negative for all x and integrates to one; therefore, it is a valid probability density. We remark that squaring the polynomial factor secures non-negativity but changes the relationship between the parameters (μ_3, μ_4) and the raw moments of f; in particular, the raw third and fourth moments of f are no longer equal to the input values (μ_3, μ_4) in general, and must be computed from f if desired. □

Appendix C. Moments of the Normalized SKTE Density

This appendix provides explicit formulas for the model-implied third and fourth raw moments of the normalized Skew–Kurtotic t Expansion (SKTE) density:

$$f(x; \mu_3, \mu_4, \nu) = \frac{\psi(x)^2\, t(x;\nu)}{\mathcal{Z}(\mu_3, \mu_4, \nu)}, \quad \psi(x) = 1 + \alpha_3\mu_3\varphi_3(x) + \alpha_4(\mu_4 - b_v)\varphi_4(x) \tag{A6}$$

where $t(x;\nu)$ denotes the standardized Student-t density (mean zero, variance one when defined) and where the orthogonal polynomials and constants are

$$\varphi_3(x) = x^3 - b_v x, \qquad b_v = \frac{3(\nu-2)}{\nu-4},$$

$$\varphi_4(x) = x^4 - c_2 x^2 + c_0, \qquad c_2 = \frac{6(\nu-2)}{\nu-6}, \quad c_0 = \frac{3(\nu-2)^2}{(\nu-4)(\nu-6)},$$

$$\alpha_3 = \frac{(\nu-4)^2(\nu-6)}{6(\nu-1)(\nu-2)^2}, \qquad \alpha_4 = \frac{(\nu-4)^2(\nu-6)^2(\nu-8)}{24(\nu-2)^3(\nu-1)(\nu-3)}.$$

The baseline raw moments are denoted by

$$m_r = \int_{-\infty}^{\infty} x^r t(x;\nu)\,dx, \qquad m_0 = 1.$$

The squared norms of the polynomials and the normalization constant are

$$A_3 = \int \varphi_3(x)^2 t(x;\nu)\,dx = m_6 - 2b_v m_4 + b_v^2 m_2, \tag{A7}$$

$$A_4 = \int \varphi_4(x)^2 t(x;\nu)\,dx = m_8 - 2c_2 m_6 + (c_2^2 + 2c_0) m_4 - 2c_0 c_2 m_2 + c_0^2 m_0, \tag{A8}$$

$$\mathcal{Z}(\mu_3, \mu_4, \nu) = 1 + (\alpha_3\mu_3)^2 A_3 + (\alpha_4(\mu_4 - b_v))^2 A_4. \tag{A9}$$

Appendix C.1. General Moment Expansion

Expanding $\psi(x)^2$ gives

$$\psi(x)^2 = 1 + 2\alpha_3\mu_3\varphi_3(x) + 2\alpha_4(\mu_4 - b_v)\varphi_4(x) + (\alpha_3\mu_3)^2\varphi_3(x)^2 + (\alpha_4(\mu_4 - b_v))^2\varphi_4(x)^2 + 2\alpha_3\alpha_4\mu_3(\mu_4 - b_v)\varphi_3(x)\varphi_4(x).$$

Hence, for any integer $k \geq 0$, the model-implied k-th raw moment is

$$\mathbb{E}_f[X^k] = \frac{1}{\mathcal{Z}}\Big\{ m_k + 2\alpha_3\mu_3 m_k^{(3)} + 2\alpha_4(\mu_4 - b_v) m_k^{(4)} + (\alpha_3\mu_3)^2 m_k^{(33)} + (\alpha_4(\mu_4 - b_v))^2 m_k^{(44)} + 2\alpha_3\alpha_4\mu_3(\mu_4 - b_v) m_k^{(34)} \Big\}. \tag{A10}$$

The auxiliary integrals are

$$m_k^{(3)} = \int x^k \varphi_3(x) t(x;\nu)\,dx = m_{k+3} - b_v m_{k+1}, \tag{A11}$$

$$m_k^{(4)} = \int x^k \varphi_4(x) t(x;\nu)\,dx = m_{k+4} - c_2 m_{k+2} + c_0 m_k, \tag{A12}$$

$$m_k^{(33)} = \int x^k \varphi_3(x)^2 t(x;\nu)\,dx = m_{k+6} - 2b_v m_{k+4} + b_v^2 m_{k+2}, \tag{A13}$$

$$m_k^{(44)} = \int x^k \varphi_4(x)^2 t(x;\nu)\,dx = m_{k+8} - 2c_2 m_{k+6} + (c_2^2 + 2c_0) m_{k+4} - 2c_0 c_2 m_{k+2} + c_0^2 m_k, \tag{A14}$$

$$m_k^{(34)} = \int x^k \varphi_3(x)\varphi_4(x) t(x;\nu)\,dx = m_{k+7} + (-c_2 - b_v) m_{k+5} + (c_0 + b_v c_2) m_{k+3} - b_v c_0 m_{k+1}. \tag{A15}$$

Third raw moment.

$$\begin{aligned}\mathbb{E}_f[X^3] = \frac{1}{\mathcal{Z}}\Big\{ & m_3 + 2\alpha_3\mu_3(m_6 - b_v m_4) + 2\alpha_4(\mu_4 - b_v)(m_7 - c_2 m_5 + c_0 m_3) \\ & + (\alpha_3\mu_3)^2(m_9 - 2b_v m_7 + b_v^2 m_5) \\ & + (\alpha_4(\mu_4 - b_v))^2(m_{11} - 2c_2 m_9 + (c_2^2 + 2c_0)m_7 - 2c_0 c_2 m_5 + c_0^2 m_3) \\ & + 2\alpha_3\alpha_4\mu_3(\mu_4 - b_v)(m_{10} + (-c_2 - b_v)m_8 + (c_0 + b_v c_2)m_6 - b_v c_0 m_4)\Big\}. \end{aligned} \tag{A16}$$

Fourth raw moment.

$$\begin{aligned}\mathbb{E}_f[X^4] = \frac{1}{\mathcal{Z}}\Big\{ & m_4 + 2\alpha_3\mu_3(m_7 - b_v m_5) + 2\alpha_4(\mu_4 - b_v)(m_8 - c_2 m_6 + c_0 m_4) \\ & + (\alpha_3\mu_3)^2(m_{10} - 2b_v m_8 + b_v^2 m_6) \\ & + (\alpha_4(\mu_4 - b_v))^2(m_{12} - 2c_2 m_{10} + (c_2^2 + 2c_0)m_8 - 2c_0 c_2 m_6 + c_0^2 m_4) \\ & + 2\alpha_3\alpha_4\mu_3(\mu_4 - b_v)(m_{11} + (-c_2 - b_v)m_9 + (c_0 + b_v c_2)m_7 - b_v c_0 m_5)\Big\}. \end{aligned} \tag{A17}$$

Appendix C.2. Simplification for the Standardized Symmetric t Baseline

When the baseline $t(x;\nu)$ is standardized and symmetric around zero, all odd-order moments vanish: $m_{2j+1} = 0$ for $j \geq 0$, and the variance is $m_2 = 1$. Under these conditions, the third and fourth raw moments simplify to the forms presented above. We recommend using $\nu > 12$ to ensure the existence of m_{12} and the finiteness of all terms.

$$A_3 = m_6 - 2b_v m_4 + b_v^2, \tag{A18}$$

$$A_4 = m_8 - 2c_2 m_6 + (c_2^2 + 2c_0)m_4 - 2c_0 c_2 + c_0^2, \tag{A19}$$

$$\mathcal{Z} = 1 + (\alpha_3\mu_3)^2 A_3 + \big(\alpha_4(\mu_4 - b_v)\big)^2 A_4. \tag{A20}$$

$$\begin{aligned}\mathbb{E}_f[X^3] = \frac{2\alpha_3\mu_3}{\mathcal{Z}}\Big\{ & (m_6 - b_v m_4) + \alpha_4(\mu_4 - b_v)\Big[m_{10} + (-c_2 - b_v)m_8 \\ & + (c_0 + b_v c_2)m_6 - b_v c_0 m_4\Big]\Big\}. \end{aligned} \tag{A21}$$

$$\begin{aligned}\mathbb{E}_f[X^4] = \frac{1}{\mathcal{Z}}\Big\{ & m_4 + 2\alpha_4(\mu_4 - b_v)(m_8 - c_2 m_6 + c_0 m_4) \\ & + (\alpha_3\mu_3)^2(m_{10} - 2b_v m_8 + b_v^2 m_6) \\ & + \big(\alpha_4(\mu_4 - b_v)\big)^2(m_{12} - 2c_2 m_{10} + (c_2^2 + 2c_0)m_8 - 2c_0 c_2 m_6 + c_0^2 m_4)\Big\} \end{aligned} \tag{A22}$$

It follows that the third and fourth moments of the SKTE density are explicit functions of the parameters μ_3 and μ_4 as well as the degrees of freedom ν.

For analytical convenience, the closed-form expressions of higher-order moments presented in this appendix are derived under the sufficient condition $\nu > 12$, which ensures the existence of all moments involved. This condition is imposed solely for the purpose of obtaining explicit moment formulas, and does not constitute a requirement for the empirical estimation reported in the main text.

Appendix D. Higher-Order Orthogonal Functions and the Sixth-Order SKTE Density

We work with the standardized Student-t with mean 0 and variance 1; all shown moments are under this normalization. For the sixth-order expansion, we assume $\nu > 12$.

Throughout this paper, the degrees of freedom of the Student-t distribution are denoted by ν.

For the standardized Student-t weight with degrees of freedom ν, the fifth- and sixth-order orthogonal polynomials are

$$\varphi_5(x) = x^5 - \frac{10(\nu-2)}{\nu-8}\,x^3 + \frac{15(\nu-2)^2}{(\nu-6)(\nu-8)}\,x,$$
$$\varphi_6(x) = x^6 - \frac{15(\nu-2)}{\nu-10}\,x^4 + \frac{45(\nu-2)^2}{(\nu-8)(\nu-10)}\,x^2 - \frac{15(\nu-2)^3}{(\nu-10)(\nu-8)(\nu-6)}.$$

The squared norms are

$$A_5 = \int_{-\infty}^{\infty} \varphi_5(x)^2\, t(x;\nu)\,\mathrm{d}x = \frac{120(\nu-3)(\nu-2)^4(\nu-1)}{(\nu-10)(\nu-8)^2(\nu-6)^2(\nu-4)},$$

$$A_6 = \int_{-\infty}^{\infty} \varphi_6(x)^2\, t(x;\nu)\,\mathrm{d}x = \frac{720(\nu-5)(\nu-3)(\nu-2)^5(\nu-1)}{(\nu-12)(\nu-10)^2(\nu-8)^2(\nu-6)^2(\nu-4)}.$$

We define

$$\psi_6(x) = 1 + \sum_{k=3}^{6} c_k \varphi_k(x) = 1 + c_3\varphi_3(x) + c_4\varphi_4(x) + c_5\varphi_5(x) + c_6\varphi_6(x)$$

and

$$\mathcal{Z}_6 = 1 + \sum_{k=3}^{6} c_k^2 A_k.$$

Then, the sixth-order squared-and-normalized density is

$$f_6(x; c_3, c_4, c_5, c_6, \nu) = \frac{\psi_6(x)^2\, t(x;\nu)}{\mathcal{Z}_6}.$$

For the higher-order coefficients c_5, c_6, one has the following moment-based identities (these identities express the linear expansion coefficients of g in the basis $\{\varphi_k\}$):

$$c_5 = \frac{1}{A_5}\int \varphi_5(x)\, g(x)\,\mathrm{d}x = \frac{\mu_5 + a_5\,\mu_3 + b_5\,\mu_1}{A_5},$$

$$c_6 = \frac{1}{A_6}\int \varphi_6(x)\, g(x)\,\mathrm{d}x = \frac{\mu_6 + A_6^{(c)}\,\mu_4 + B_6^{(c)}\,\mu_2 + C_6^{(c)}\,\mu_0}{A_6},$$

where

$$a_5 = -\frac{10(\nu-2)}{\nu-8}, \qquad b_5 = \frac{15(\nu-2)^2}{(\nu-6)(\nu-8)},$$

$$A_6^{(c)} = -\frac{15(\nu-2)}{\nu-10}, \quad B_6^{(c)} = \frac{45(\nu-2)^2}{(\nu-8)(\nu-10)}, \quad C_6^{(c)} = -\frac{15(\nu-2)^3}{(\nu-10)(\nu-8)(\nu-6)}.$$

Under standardization $\mu_1 = 0,\ \mu_2 = 1,\ \mu_0 = 1$, these simplify to

$$c_5 = \frac{\mu_5 + a_5\,\mu_3}{A_5}, \qquad c_6 = \frac{\mu_6 + A_6^{(c)}\,\mu_4 + B_6^{(c)} + C_6^{(c)}}{A_6}.$$

https://doi.org/10.3390/sym18020301

Note: The above moment identities

$$c_5 = \frac{1}{A_5}\int \varphi_5(x)\, g(x)\, \mathrm{d}x, \qquad c_6 = \frac{1}{A_6}\int \varphi_6(x)\, g(x)\, \mathrm{d}x$$

represent the coefficients of the linear expansion $g(x) = \sum_r c_r\, \varphi_r(x)\, t(x;\nu)$. When the squared-and-normalized form $f_6(x) = \psi_6(x)^2\, t(x;\nu)/\mathcal{Z}_6$ is adopted, the mapping from moments (or sample moments) to the coefficients c_k becomes nonlinear; thus, these identities do not hold exactly for the c_k appearing in f_6. In empirical use, the parameters c_k in f_6 should be estimated by maximum likelihood or numerical fitting (e.g., least squares on density or quantile targets). To ensure numerical stability, one should avoid denominator roots in A_5 and A_6; in practice, $\nu > 10$ is recommended for A_5 and $\nu > 12$ for A_6.

References

1. Falk, M. Asymptotic independence of median and MAD. *Stat. Probab. Lett.* **1997**, *34*, 341–345. [CrossRef]
2. Giona, M.; Pezzotti, C.; Procopio, G. Another normality is possible. Distributive transformations and emergent Gaussianity. *Phys. A* **2024**, *634*, 129450. [CrossRef]
3. Millington, T.; Niranjan, M. Construction of minimum spanning trees from financial returns using rank correlation. *Phys. A* **2021**, *566*, 125605. [CrossRef]
4. Takaishi, T. Bias correction in the realized stochastic volatility model for daily volatility on the Tokyo Stock Exchange. *Phys. A* **2018**, *500*, 139–154. [CrossRef]
5. Chin, W.C. Heavy-tailed value-at-risk analysis for Malaysian stock exchange. *Phys. A* **2008**, *387*, 4285–4298. [CrossRef]
6. Begušić, S.; Kostanjčar, Z.; Stanley, H.E.; Podobnik, B. Scaling properties of extreme price fluctuations in Bitcoin markets. *Phys. A* **2018**, *510*, 400–406. [CrossRef]
7. Cortés, L.M.; Mora-Valencia, A.; Perote, J. Measuring firm size distribution with semi-nonparametric densities. *Phys. A* **2017**, *485*, 35–47. [CrossRef]
8. Kim, J.H.; Kim, H. Estimating Skewness and Kurtosis for Asymmetric Heavy-Tailed Data: A Regression Approach. *Mathematics* **2025**, *13*, 2694. [CrossRef]
9. Wampler, T.; Barato, A.C. Skewness and kurtosis in stochastic thermodynamics. *J. Phys. Math. Theor.* **2021**, *55*, 014002. [CrossRef]
10. Del Brio, E.B.; Mora-Valencia, A.; Perote, J. Semi-nonparametric VaR forecasts for hedge funds during the recent crisis. *Phys. A* **2014**, *401*, 330–343. [CrossRef]
11. Li, H.; Xu, Y.; Yue, X.; Kurths, J. Transition-event duration in one-dimensional systems under correlated noise. *Phys. A* **2019**, *532*, 121764. [CrossRef]
12. Jiménez, I.; Mora-Valencia, A.; Perote, J. Dynamic selection of Gram-Charlier expansions with risk targets: An application to cryptocurrencies. *Risk Manag.* **2022**, *24*, 81–99. [CrossRef]
13. Jiang, X.; Cheng, L.; Dai, X. The effects of skewness and kurtosis on production and hedging decisions: A Gram-Charlier expansion approach. *Financ. Innov.* **2025**, *11*, 70. [CrossRef]
14. Jondeau, E.; Poon, S.H.; Rockinger, M. *Financial Modeling under Non-Gaussian Distributions*; Springer Science & Business Media: London, UK, 2007.
15. Jondeau, E.; Rockinger, M. Conditional volatility, skewness, and kurtosis: Existence, persistence, and comovements. *J. Econ. Dyn. Control* **2003**, *27*, 1699–1737. [CrossRef]
16. Jurczenko, E.; Maillet, B.; Merlin, P. Hedge Fund Portfolio Selection with Higher-order Moments: A Nonparametric Mean–Variance–Skewness–Kurtosis Efficient Frontier. In *Multi-moment Asset Allocation and Pricing Models*; Jurczenko, E., Maillet, B., Eds.; John Wiley & Sons: Chichester, UK, 2006; pp. 51–66. [CrossRef]
17. Peng, S. *A Study of Portfolio Optimization Based on Higher-Order Moments*; China Forestry Press: Beijing, China, 2016. (In Chinese)
18. Azzalini, A.; Capitanio, A. *The Skew-Normal and Related Families*; Cambridge University Press: Cambridge, UK, 2014; Volume 3.
19. Jondeau, E.; Rockinger, M. Gram-Charlier densities. *J. Econ. Dyn. Control* **2001**, *25*, 1457–1483. [CrossRef]
20. Stuart, A.; Ord, K. *Kendall's Advanced Theory of Statistics*; Hodder Arnold: London, UK, 1994.
21. Berberan-Santos, M.N. Expressing a probability density function in terms of another PDF: A generalized Gram-Charlier expansion. *J. Math. Chem.* **2007**, *42*, 585–594. [CrossRef]
22. Gallant, A.R.; Tauchen, G. Seminonparametric estimation of conditionally constrained heterogeneous processes: Asset pricing applications. *Econometrica* **1989**, *57*, 1091–1120. [CrossRef]
23. León, Á.; Rubio, G.; Serna, G. Autoregresive conditional volatility, skewness and kurtosis. *Q. Rev. Econ. Financ.* **2005**, *45*, 599–618. [CrossRef]
24. Li, Q.; Wang, N.; Yi, D. *Numerical Analysis*; Tsinghua University Press: Beijing, China, 2008. (In Chinese)

25. Xu, X.; Wang, R.; Gu, B. The high-order moments of the three major statistical distributions and their applications. *Stat. Decis.* **2015**, *23*, 66–69. (In Chinese) [CrossRef]
26. Cramér, H. *Mathematical Methods of Statistics*; Princeton University Press: Boston, MA, USA, 1999.
27. Yahoo Finance. Yahoo Finance Database. 2025. Available online: https://finance.yahoo.com (accessed on 10 September 2025).

Disclaimer/Publisher's Note: The statements, opinions and data contained in all publications are solely those of the individual author(s) and contributor(s) and not of MDPI and/or the editor(s). MDPI and/or the editor(s) disclaim responsibility for any injury to people or property resulting from any ideas, methods, instructions or products referred to in the content.